# Improved performance of ceria-based solid oxide fuel cell using doped LaGaO$_3$ films deposited by pulsed laser deposition

Jing Qian [a], Zhiwen Zhu [a], Guoshun Jiang [a], Wei Liu [a,b,*]

[a] CAS Key Laboratory of Materials for Energy Conversion, Department of Materials Science and Engineering, University of Science and Technology of China, Hefei 230026, China
[b] Key Laboratory of Materials Physics, Institute of Solid State Physics, Chinese Academy of Sciences, Hefei 230031, China

## HIGHLIGHTS

- Fabricate thin LSGM layer on SDC half-cell with pulsed laser deposition.
- The thin LSGM layer blocks electronic current in SDC layer.
- The bilayer cell retains the chemical, mechanical and structural integrity.
- The electrochemical performance and OCVs of the cell have been improved.

## ARTICLE INFO

## ABSTRACT

A dense La$_{0.9}$Sr$_{0.1}$Ga$_{0.8}$Mg$_{0.2}$O$_{3-\delta}$ (LSGM) film is fabricated using the pulsed laser deposition (PLD) technique on a Ce$_{0.8}$Sm$_{0.2}$O$_{2-\delta}$ (SDC) electrolyte which is prepared using a co-pressing process on a NiO–SDC anode substrate. The LSGM/SDC bilayer electrolyte cell with Sm$_{0.5}$Sr$_{0.5}$CoO$_{3-\delta}$–Ce$_{0.8}$Sm$_{0.2}$O$_{2-\delta}$ (SSC–SDC, 70:30 wt.%) cathode achieves significantly enhanced cell performance, yielding open circuit voltage (OCV) value of 0.89 V and maximum power density of 758 mW cm$^{-2}$ at 700 °C. The electrical current leakage in the SDC single layer cell caused by the reduction of Ce$^{4+}$ to Ce$^{3+}$ in reducing environment has been eliminated by depositing the LSGM thin film as a blocking layer; besides, the reaction between NiO and LSGM can be prevented due to the dense SDC electrolyte layer. The influence of oxygen pressure and post-annealing temperature on the crystallinity, microstructure and surface roughness of the LSGM films are studied for obtaining a high quality film. Characterization analysis of the cell shows that the bilayer electrolyte deposited by the PLD technique have retained the chemical, mechanical and structural integrity of the cell.

## 1. Introduction

Solid oxide fuel cells (SOFCs) can directly convert stored chemical energy to usable electrical energy and overcome combustion efficiency limitation [1]. The main barrier for the wide application of SOFCs technology is its high operating temperature (900–1000 °C) [2]. Lowering the operating temperature can prolong cell component lifetime, slower degradation rate and allow wider selection of low cost interconnects materials [3]. However, as the operating temperature decreases, the cell performance falls sharply due to the increase in internal resistance [4]. Several electrolyte materials with high ionic conductivity, such as samaria-doped ceria (SDC) [5] and lanthanum strontium gallate magnesite (LSGM) [6], have been studied for intermediate temperature SOFCs. SDC is considered to be one of the most promising materials for SOFCs, and its conductivity is 2–3 times higher than that of yttria-stabilized zirconia (YSZ) [7]. However, the reduction of Ce$^{4+}$ to Ce$^{3+}$ causes SDC to exhibit n-type conductivity, which results in low open circuit voltages (OCVs) of the fuel cell. LSGM has been identified as a superior oxide-ion electrolyte for intermediate-temperature SOFCs due to its high chemical stability, negligible electronic conductivity and high ionic conductivity over a wide range of oxygen partial pressures [8–10]. The disadvantage of the LSGM electrolyte is the chemical reaction between LSGM and the traditionally used anode catalyst Ni at high temperatures [11,12].

* Corresponding author. CAS Key Laboratory of Materials for Energy Conversion, Department of Materials Science and Engineering, University of Science and Technology of China, Hefei 230026, China. Tel.: +86 551 63606929; fax: +86 551 63602586.
E-mail address: wliu@ustc.edu.cn (W. Liu).

The problems can be eliminated by incorporating LSGM as a blocking layer between the SDC electrolyte and cathode. The LSGM layer can inhibit electronic current leakage of the SDC electrolyte, while the dense SDC layer can prevent the reaction between LSGM and NiO. In previous studies, various techniques have been devoted to fabricating the LSGM layer, such as tape casting [9], doctor blade [13] and screen printing method [14]. However, these processes normally require processing temperatures over 1300 °C. At such high co-sintering temperatures, lanthanum (La) may diffuse from LSGM to SDC layer and form La-doped $CeO_2$ (LDC) which has lower oxygen ion conductivity than that of SDC [15]. The pulsed laser deposition (PLD) technique can operate at low processing temperature (below 800 °C) without high post-annealing temperature [16], which can avoid La diffusion and is useful for low-temperature SOFC applications. Furthermore, the PLD technique is a promising method that offers better control of the deposited film properties, such as microstructures, density and stoichiometric with multi-component materials [2,17]. In this work, we deposited a LSGM thin layer on a SDC electrolyte cell using the PLD technique to block electron conduction. The electrochemical performances and properties of the bilayer electrolytes cells with $Sm_{0.5}Sr_{0.5}CoO_{3-\delta}$–$Ce_{0.8}Sm_{0.2}O_{2-\delta}$ composite cathode were tested and characterized in the research. To get a deeper understanding of the growth mechanism and microstructure properties correlation in the LSGM films, we investigated the effect of the oxygen partial pressures during the PLD technique and the post-annealing temperatures along with morphological, structural and compositional characterization. The electrochemical performance of the bilayer electrolyte cells was also discussed in details.

## 2. Experimental

### 2.1. Powder synthesis and cell fabrication

SDC powders were fabricated using a citric acid-nitrate gel combustion process [18]. First, $Sm_2O_3$ and $Ce(NO_3)_3 \cdot 6H_2O$ was added to a solution of $HNO_3$. After the solution became clear, citric acid was added in a 1:1.5 metal ions: citric acid molar ratio. The pH value was adjusted to approximately 7 with ammonia. The solution was continuously stirred and heated at 70 °C until a gel formed. The gel was then heated on a hot plate and combusted to form powder precursors, which were then calcined at 600 °C for 3 h to obtain a pure, crystalline SDC phase. NiO–SDC anode substrate was prepared by uniaxially press method. NiO ($NiCO_3 \cdot 2Ni(OH)_2 \cdot 4H_2O$ decomposed at 600 °C), SDC powders in a weight ratio of 60:40 with 10 wt.% starch as pore formers were mixed in ethanol and ball-milled for 24 h. The anode supporting half-cells were fabricated using the co-pressing method. The NiO–SDC mixed powders were uniaxially pressed to form anode supports with a certain mechanical strength. Then, the as-prepared SDC powders were well distributed and pressed on the anode substrates to fabricate the SDC electrolyte layer. Finally, the anode supporting half-cells were sintered at 1400 °C for 5 h.

The LSGM thin layer was fabricated by ablating a LSGM target (fabricated by solid-state reaction [9] and sintered at 1500 °C for 5 h) with a KrF excimer laser ($\lambda = 248$ nm) at a repetition rate of 10 Hz and the laser energy density adjusted to 3 J cm$^{-2}$. The SDC half-cells substrate were heated at 600 °C. Oxygen gas was flowed into the chamber in a constant flux during deposition with pressures adjusted to range from 0.067 Pa to 10 Pa. The post-annealing temperatures of the deposited film was ranging from 800 to 1150 °C.

$Sm_{0.5}Sr_{0.5}CoO_{3-\delta}$–$Ce_{0.8}Sm_{0.2}O_{2-\delta}$ (SSC–SDC) as the cell cathode, which was composed of composite powders mixed with a 10 wt.% ethylcellulose-terpineol binder, was painted on the bilayer electrolytes and then fired at 1000 °C for 3 h to form a complete cell. Ag paste was applied on the electrode as a current collector.

### 2.2. Cell tests

The electrochemical performance characteristics of the cells were evaluated with an $Al_2O_3$ test housing placed inside of a furnace. The cell testing was performed from 550 to 700 °C with humidified hydrogen (∼3% $H_2O$) as a fuel and atmospheric air as the oxidant. The flow rate of the humidified hydrogen was 25 mL min$^{-1}$. The performance was measured with a DC Electronic Load (ITech Electronics model IT8511). The resistances of the cell under open circuit conditions were measured with an impedance analyzer (CHI604B, Shanghai Chenhua), and the frequency was swept from 100 kHz to 0.1 Hz.

### 2.3. Characterization of phase composition and microstructures of the cells

The crystal structures of deposited LSGM films were examined using an X-ray diffractometer (XRD) equipped with Cu Kα radiation. The surface microstructures of films were observed with a scanning electron microscope (SEM, JEOL JSM-6700F), and the elemental distribution was determined using energy-dispersive X-ray spectroscopy (EDS). Atomic force microscopy (AFM, Innova) measurements were performed to characterize the surface and to measure the roughness of the deposited LSGM films.

## 3. Results and discussion

### 3.1. Influence of oxygen pressure

The effects of oxygen partial pressure on the microstructure of the deposited LSGM films in deposition procedure were discussed. The AFM micrographs of the LSGM films deposited at different oxygen partial pressures are shown in Fig. 1. The root-mean-squared (RMS) roughness of the LSGM films deposited at oxygen pressure of 0.067, 0.67, 3 and 10 Pa are 29.7, 34.5, 28.3 and 32.8 nm, respectively. The RMS of the LSGM films is larger than that of other films deposited by PLD [19,20], and this is mainly caused by the roughened surface of the SDC films. Thus, it is necessary to polish the SDC films to obtain a smoother surface. The diffusion coefficient of adatoms is correlated with oxygen pressure during the PLD process. The low oxygen pressure results in high diffusion coefficient of adatoms and low density of nuclei [21]. As shown in Fig. 1a and b, the increase of RMS roughness with increase of oxygen pressure (from 0.067 Pa to 0.67 Pa) is attributed to the larger grain size which could be the effect of enhanced vapor-phase condensation and coalescence of particulates during their transit from target to substrate [22]. As the oxygen pressure increases, the evaporated particulates from the ablated target were condensed and coalesced before deposited on the substrate. Besides, higher oxygen pressure results in an increased nuclei density and thus generates larger size grain. When the oxygen pressure increases to 3 Pa as shown in Fig. 1c, the oxygen molecules slower the rate of laser plume towards the substrate and gives the adatoms greater mobility on the surface, thereby decreasing the roughness of the films. However, more oxygen molecules will impede the expansion of the laser-produced vapor plume. This interaction will decrease the plume energy and reduce the average energy of the ions deposition onto the substrate. In the end, it will roughen the surface of the deposited film which is depicted in Fig. 1d. Ishihara et al. [4] have reported that the composition of LSGM films deposited by the PLD technique is nearly independent of the oxygen pressure at low oxygen pressure region. However, the composition of the LSGM
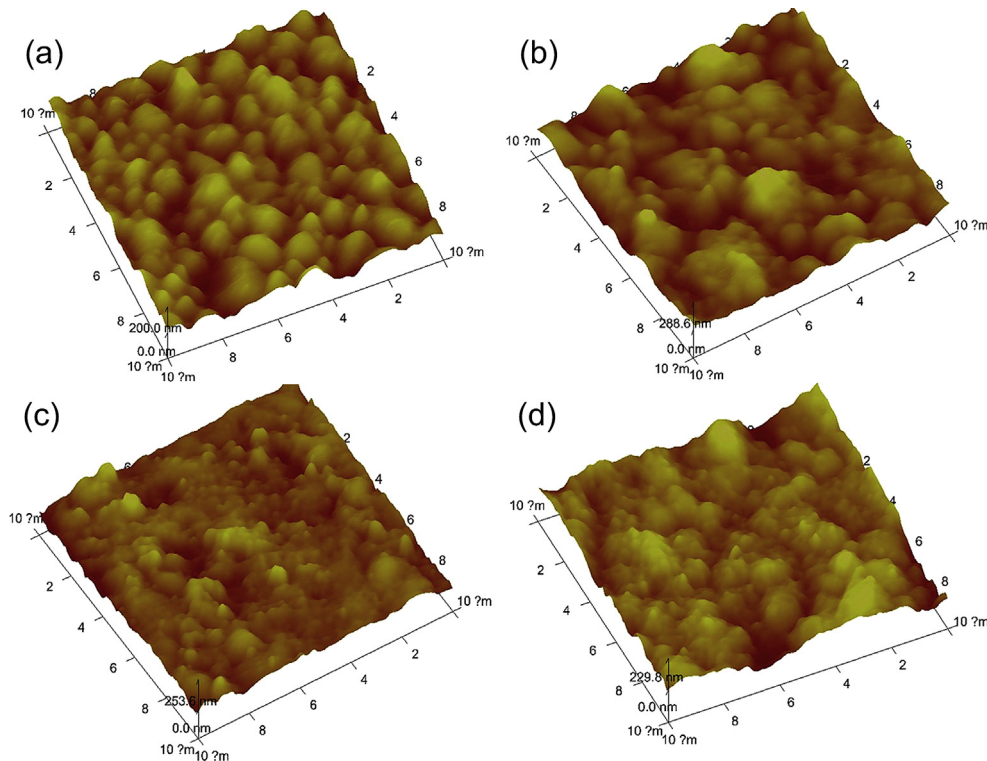
**Fig. 1.** The AFM micrographs of the LSGM films deposited at different oxygen partial pressure of: (a) 0.067 Pa, (b) 0.67 Pa, (c) 3 Pa and (d) 10 Pa.

film deviates drastically when the pressure is higher than 0.1 Pa. The compositions of the LSGM films deposited at different temperatures were determined using energy-dispersive X-ray spectroscopy (EDS). The atomic composition of La, Sr, Ga and Mg at oxygen pressure of 10 Pa is 48.17%, 11.67%, 30.71% and 9.45%, respectively. These values correspond to the film composition $La_{0.80}Sr_{0.20}Ga_{0.76}Mg_{0.24}O_{3-\delta}$ which deviates from that of the target $La_{0.9}Sr_{0.1}Ga_{0.8}Mg_{0.2}O_{3-\delta}$. Similarly, the compositions of other three films are estimated to be $La_{0.86}Sr_{0.14}Ga_{0.83}Mg_{0.17}O_{3-\delta}$, $La_{0.87}Sr_{0.13}Ga_{0.81}Mg_{0.19}O_{3-\delta}$ and $La_{0.86}Sr_{0.14}Ga_{0.79}Mg_{0.21}O_{3-\delta}$ at the oxygen pressure of 3, 0.67 and 0.067 Pa, respectively. The compositions of the films deposited at 0.67 and 0.067 Pa are nearly consistent with that of the target. The oxygen pressure in the PLD process was kept at 0.67 Pa in our study.

### 3.2. Influence of post-annealing temperature

Fig. 2 shows the X-ray diffraction patterns of the as-grown LSGM films deposited at oxygen pressure of 0.67 Pa and the films post annealed at different temperatures. No reflection of the LSGM phase is found in the film deposited at 700 °C, indicating the amorphous state [23,24]. The amorphous phase is mainly caused by the complicated stoichiometry of the LSGM composition and the relative low temperature of the substrate in deposition procedure [25]. The latter reason can be explained by the sluggish kinetics of crystal growth at relative low substrate temperature during film deposition. The relative low substrate temperature cannot afford enough mobility for the atoms to arrive at the substrate from the laser ablation plume and thus those atoms become immobilized when they land on the substrate [25,26]. The phenomenon can be improved with increasing substrate temperature [27]. However, due to the limitation of our equipment setting, we cannot make further improvement on the substrate temperature, thus we did

not discuss the influence of substrate temperature on the structure of the deposited films. In order to solve the amorphous state of the deposited films, the deposited LSGM films were post-annealed to improve the crystallinity. When the deposited LSGM film annealed at 800 °C, the XRD pattern shows mixture of phases as depicted in Fig. 2. The crystalline structures such as $La_4Ga_2O_9$, $LaSrGaO_4$, $LaSrGa_3O_7$ are observed in the annealed film. After annealed at 1000 °C, the LSGM film shows the basic structure of $LaGaO_3$ oriented in the (110) direction. The impurity phases also exist with much lower intensity. When the annealing temperature increases to 1150 °C, further crystallized film into the LSGM phase, leaving the unwanted
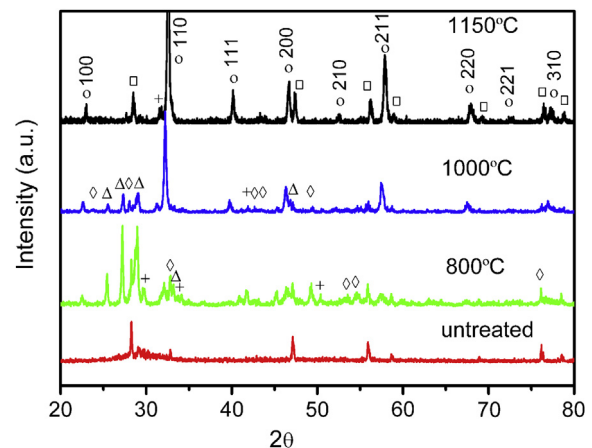


**Fig. 2.** The X-ray diffraction patterns of the as-grown LSGM films at oxygen pressure of 0.67 Pa and the deposited LSGM films after post-annealing at different temperatures: (○) $LaGaO_3$, (□) $Ce_{0.8}Sm_{0.2}O_2$, (+) $LaSrGa_3O_7$, (△) $La_4Ga_2O_9$, (◇) $LaSrGaO_4$.

secondary peaks exist in Fig. 2. The surface morphology of the as-deposited LSGM film and the post-annealed LSGM films at different temperatures are depicted in Fig. 3. It can be seen that the LSGM film deposited on the SDC half-cell in Fig. 3a is fully dense, uniform and continuous with no cracks or pin-holes. Fig. 3b shows the surface of the LSGM film annealed at 800 °C. It seems dense and no obvious change of grain size appears. After post-annealed at 1000 °C, the grain structure of the LSGM film seems a little change from that of the as-deposited film as shown in Fig. 3c. When the post-annealed temperature increases to 1150 °C, the surface morphology of the LSGM film changes apparently as depicted in Fig. 3d. The AFM micrographs of the LSGM films post-annealed at different temperatures are shown in Fig. 4. The RMS roughness of the LSGM films are (a) 61.5, (b) 51.6 and (c) 36.1 nm at 800, 1000 and 1150 °C, respectively. The RMS roughness of the LSGM film annealed at 800 °C is larger than the as-grown film (34.5 nm) without annealing, indicating the crystallization formation in annealing process. With the increase of annealing temperature to 1000 °C and 1150 °C, the surface roughness decreases. This can be understood because higher annealing temperatures provide more thermal energy to activate atom diffusion and hence facilitate the repairing of dislocated atomic occupancies. These post-annealed LSGM films were painted with the SSC-SDC cathode and tested with humidified hydrogen (3% $H_2O$) as a fuel and atmospheric air as an oxidant. Fig. 5a presents the cell performances of the LSGM/SDC bilayer electrolytes cells operated at 700 °C with LSGM films annealed at 800 °C and 1150 °C. The bilayer electrolytes cell with LSGM annealed at 1150 °C exhibits the open circuit voltage (OCV) of 0.727 V which is lower than the single SDC electrolyte cell [28]. The cell with LSGM film annealed at 800 °C exhibits the OCV of 0.781 V at 700 °C. It shows a small increase in the OCV compared with the SDC single cell. The compositions of the LSGM films after annealed at 800 °C and 1150 °C are $La_{0.86}Sr_{0.14}Ga_{0.76}Mg_{0.24}O_{3-\delta}$ and $La_{0.88}Sr_{0.12}Ga_{0.74}Mg_{0.26}O_{3-\delta}$, respectively, which deviate from the as-deposited LSGM film. Although the higher annealing temperature can improve the purity of LSGM pervoskite structure and

decrease the roughness of films, it can accelerate the volatilization of Ga element in the LSGM film and thus influence the cell performance. Fig. 5b shows the $I-V$ characteristics and power densities of the LSGM/SDC bilayer electrolytes cell operated at 550−700 °C. The as-grown LSGM film was painted with the SSC−SDC cathode and fired at 1000 °C. The firing process of the cathode onto the LSGM/SDC bilayer electrolytes contains the post-annealing process of LSGM film and thus the technique procedures can be simplified. Besides, the one-step annealing and firing process can decrease the extent of volatilization. As shown in Fig. 5b, the OCV achieves to 0.89, 0.903, 0.91 and 0.919 V at 700, 650, 600 and 550 °C, respectively. The high OCV value indicates that the electronic current through the ceria-based electrolyte is effectively and mostly blocked and few defects, such as cracks and pin-holes, are existed in the LSGM/SDC bilayer electrolytes or at the interface. Nevertheless, the OCV of the LSGM/SDC bilayer electrolytes cell is still lower than the typical LSGM cell. It is reported that only with a proper thickness ratio of the bilayer electrolytes can increase the interfacial oxygen partial pressure and thus reduces the n-type conductivity of SDC and decreases the penetration electronic current through the bilayer and thus leads to an increase in the OCV [29,30]. Therefore, further improvement in the thickness ratio is needed to be discussed to obtain higher OCVs. Besides, the unwanted phases, such as $LaSrGaO_4$, $LaSrGa_3O_7$, exist in the LSGM film and cause the cell OCV lower than the theoretical value. Fig. 5b shows the maximum power densitites of the cell increase to 758, 616, 478 and 262 mW cm$^{-2}$ at 700, 650, 600 and 550 °C, respectively. Fig. 5c depicts the electrochemical impedance spectra of the LSGM/SDC bilayer electrolytes cell without post-annealing process. The inset shows the spectrum of the SDC single layer cell. The first intercept on the real axis at high frequency corresponds to the ohmic resistance (Ro), which includes internal resistance of the electrolyte and electrodes and the contact resistance at the interfaces between the electrodes and the electrolytes and between the electrodes and the current collectors [31]. The difference between the high frequency and the low frequency represents the interfacial polarization
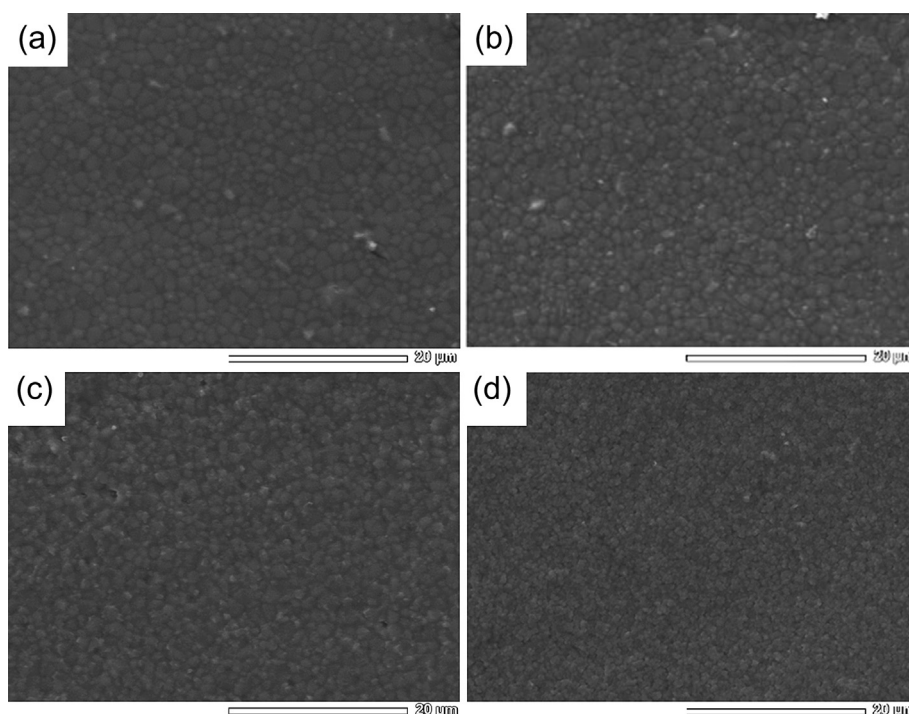


**Fig. 3.** The surface morphology of (a) the deposited LSGM film, the as-grown LSGM films post-annealed at: (b) 800 °C, (c) 1000 °C, (d) 1150 °C.
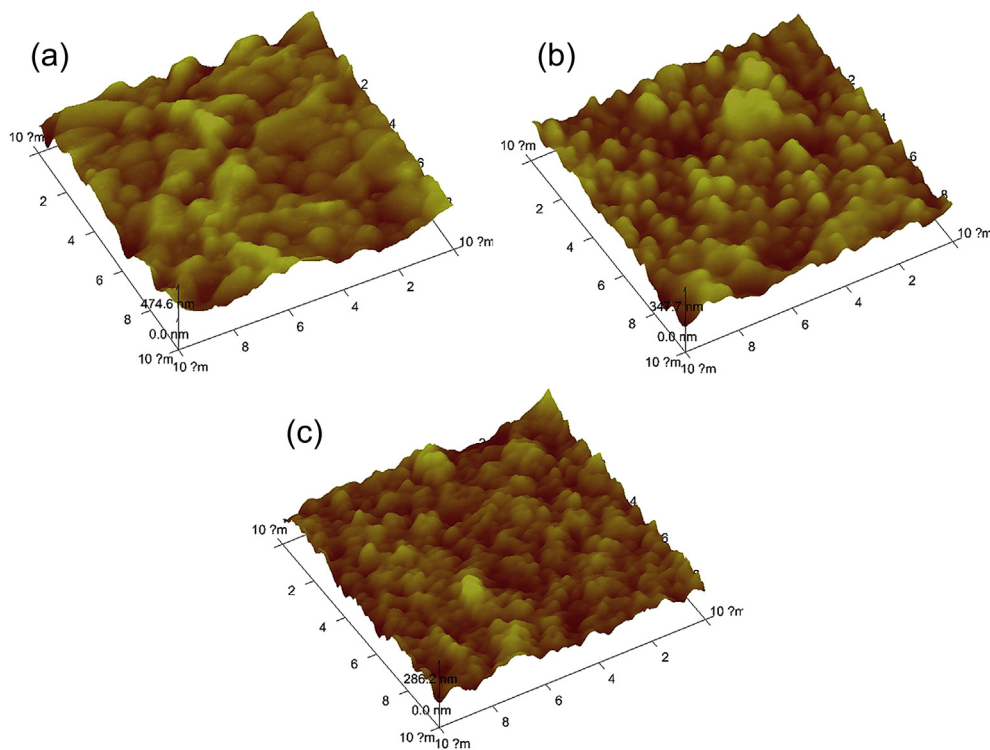
**Fig. 4.** The AFM micrographs of the LSGM films post-annealed at: (a) 800 °C, (b) 1000 °C, (c) 1150 °C.

resistance (Rp), which is contributed by cathode and anode [32]. The ohmic resistance (Ro) is almost the same for the two cells, which implies that the addition of the LSGM thin layer has little effect on the resistance of the electrolyte. However, the polarization resistance (Rp) increases from 0.05, 0.07, 0.15, 0.38 $\Omega$ cm$^2$ in SDC single cell to 0.12, 0.17, 0.35 and 0.75 $\Omega$ cm$^2$ in LSGM/SDC bilayer electrolyte cell at 700, 650, 600, and 550 °C, respectively. The poor adhesion between the PLD LSGM layer and the painted cathode can
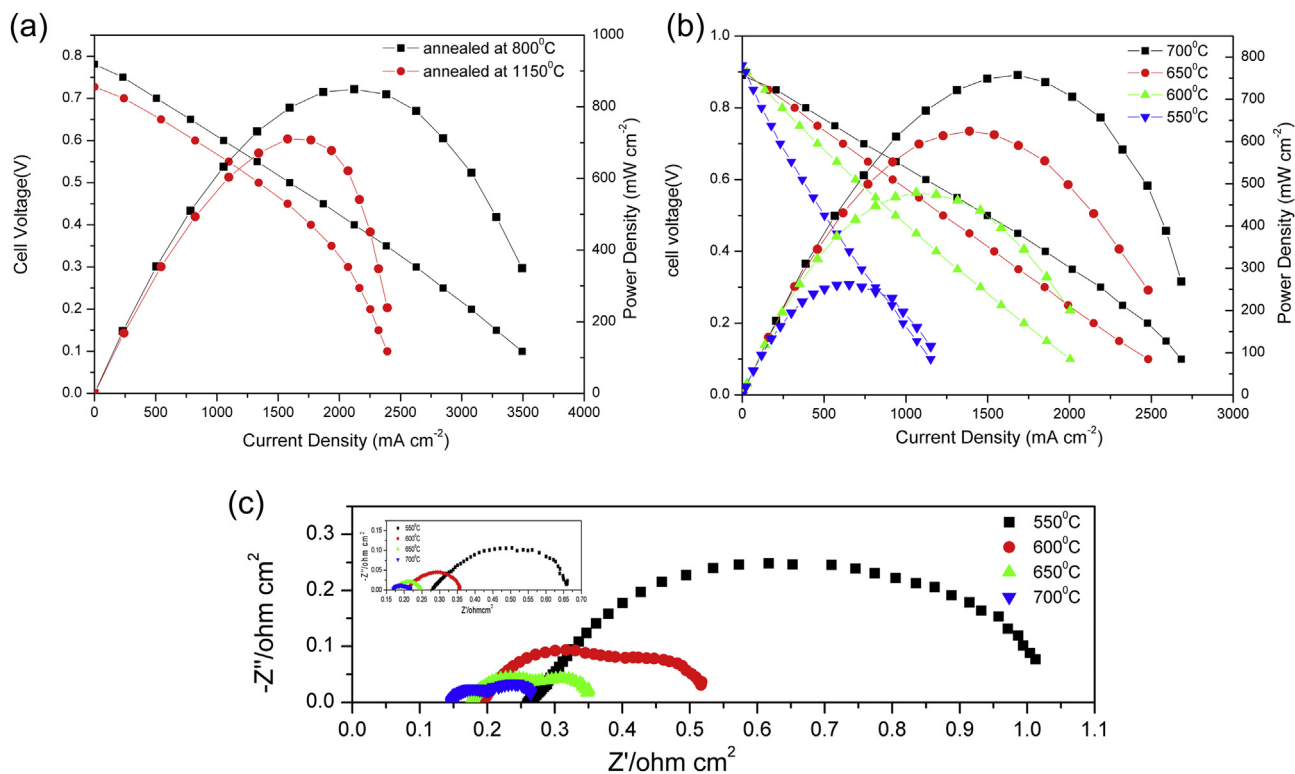


**Fig. 5.** (a) The cell voltage and power density versus current density for LSGM/SDC bilayer electrolytes cells operated at 700 °C with LSGM films annealed at 800 °C and 1150 °C; (b) The I−V characteristics and power densities of the LSGM/SDC bilayer electrolytes cell operated at 550−700 °C without post-annealing process; (c) The electrochemical impedance spectra of the LSGM/SDC bilayer electrolytes cell operated at 550−700 °C without post-annealing process. The inset shows the spectrum of the SDC single layer cell.

impact the cathodic performance [33]. Further improvements in optimizing the microstructure of the electrode are also expected to improve the performance of the cell. The high cell performance shows that no interfacial reaction between LSGM and Ni-based anode is occurred because of the low deposition temperature of PLD technique. The LSGM thin film can block electronic conduction in SDC electrolyte, while the dense SDC electrolyte can prevent the reaction between LSGM and NiO. The LSGM/SDC bilayer electrolyte cell enable the superior chemical, mechanical and structural stability in the cell.

## 4. Conclusions

PLD technique has been used in this study to deposit the LSGM electronic blocking layer on SDC half-cell with PLD technique. We have investigated the influence of deposition and post-annealing parameters on the surface morphology, roughness and orientation of the LSGM films deposited on SDC half-cell. In terms of the quality, deposition rate and composition of the LSGM film deposited by PLD technique, the proper oxygen pressure seems to be 0.67 Pa. In order to improve the crystallinity of the deposited LSGM films, the suitable method is the one-step process which means keeping the cathode firing and the post-annealing procedure in the same process. Interfacial reaction between LSGM and Ni-based anode was avoided due to the low processing temperatures of the PLD technique. The OCVs of the LSGM (∼2 μm)/SDC (∼22 μm) bilayer electrolytes cell are 0.89, 0.903, 0.91 and 0.919 V at 700, 650, 600 and 550 °C, respectively which indicates the effectiveness of LSGM as an electron blocking layer. The maximum power densities of 758, 616, 478 and 262 mW cm$^{-2}$ with the polarization resistances of 0.12, 0.17, 0.35 and 0.75 Ω cm$^2$ were achieved at 700, 650, 600 and 550 °C, respectively. The proper cathode and rough surface of deposited films may result in the optimum cell performance and this problem will be discussed in our future plan. Compared with other wet ceramic processes which require high processing temperatures, PLD method proves to be a prospective technique with low processing temperature for depositing high quality thin layer for SOFCs. The LSGM/SDC bilayer electrolytes SOFC deposited by PLD technique presents a feasible structure for enhancing a superior cell performance and enabling mechanical integrity and better thermo-mechanical stability of the cells.

## Acknowledgments

## References

[1] E.D. Wachsman, K.T. Lee, Science 334 (2011) 935–939.
[2] D. Yang, X. Zhang, S. Nikumb, C. Deces-Petit, R. Hui, R. Maric, D. Ghosh, Journal of Power Sources 164 (2007) 182–188.
[3] L. Zigui, J. Hardy, J. Templeton, J. Stevenson, D. Fisher, W. Naijuan, A. Ignatiev, Journal of Power Sources 210 (2012) 292–296.
[4] J.W. Yan, H. Matsumoto, T. Akbay, T. Yamada, T. Ishihara, Journal of Power Sources 157 (2006) 714–719.
[5] H. Uchida, S. Arisaka, M. Watanabe, Electrochemical and Solid State Letters 2 (1999) 428–430.
[6] F. Bozza, R. Polini, E. Traversa, Fuel Cells 8 (2008) 344–350.
[7] T. Shimonosono, Y. Hirata, Y. Ehira, S. Sameshima, T. Horita, H. Yokokawa, Solid State Ionics 174 (2004) 27–33.
[8] Z. Zhan, D. Han, T. Wu, X. Ye, S. Wang, T. Wen, S. Cho, S.A. Barnett, RSC Advances 2 (2012) 4075–4078.
[9] X.-d. Zhu, N.-q. Zhang, L.-j. Wu, K.-n. Sun, Y.-x. Yuan, Journal of Power Sources 195 (2010) 7583–7586.
[10] N. Yang, A. D'Epifanio, E. Di Bartolomeo, C. Pugnalini, A. Tebano, G. Balestrino, S. Licoccia, Journal of Power Sources 222 (2013) 10–14.
[11] W. Guo, J. Liu, C. Jin, Journal of Alloys and Compounds 504 (2010) L21–L24.
[12] Y.-W. Ju, S. Ida, T. Inagaki, T. Ishihara, Journal of Power Sources 196 (2011) 6062–6069.
[13] L. Xuejiao, M. Xie, H. Da, W. Hao, Z. Fanrong, Z. Zhongliang, Journal of Power Sources 222 (2013) 92–96.
[14] J.-E. Hong, T. Inagaki, T. Ishihara, Ionics 18 (2012) 433–439.
[15] Y.-W. Ju, T. Inagaki, S. Ida, T. Ishihara, Journal of the Electrochemical Society 158 (2011) B825–B830.
[16] D. Pergolesi, E. Fabbri, E. Traversa, Electrochemistry Communications 12 (2010) 977–980.
[17] J.H. Joo, G.M. Choi, Solid State Ionics 177 (2006) 1053–1057.
[18] W. Sun, Y. Jiang, Y. Wang, S. Fang, Z. Zhu, W. Liu, Journal of Power Sources 196 (2011) 62–68.
[19] S.K. Pandey, O.P. Thakur, R. Raman, A. Goyal, A. Gupta, Applied Surface Science 257 (2011) 6833–6836.
[20] D. Hong, L. Liu, X. Song, Y. Li, Journal of Superconductivity and Novel Magnetism 24 (2011) 1707–1713.
[21] X.Z. Liu, S.M. He, D.H. Li, Q.F. Lu, Z.H. Wang, S.X. Bao, Y.R. Li, Journal of Materials Science 40 (2005) 5139–5145.
[22] L. Lei, X. Dingquan, L. Dunmin, Z. Yongbin, Z. Jianguo, Physica B 404 (2009) 325–328.
[23] S. Kanazawa, T. Ito, K. Yamada, T. Ohkubo, Y. Nomoto, T. Ishihara, Y. Takita, Surface & Coatings Technology 169 (2003) 508–511.
[24] S. Heiroth, T. Lippert, A. Wokaun, M. Doebeli, J.L.M. Rupp, B. Scherrer, L.J. Gauckler, Journal of the European Ceramic Society 30 (2010) 489–495.
[25] T. Rojo, I.R. de Larramendi, R.L. Anton, J.I.R. de Larramendi, S. Baliteau, F. Mauvy, J.C. Grenier, Journal of Power Sources 169 (2007) 35–39.
[26] T. Mathews, J.R. Sellar, B.C. Muddle, P. Manoravi, Chemistry of Materials 12 (2000) 917–922.
[27] J.H. Shim, J.S. Park, J. An, T.M. Guer, S. Kang, F.B. Prinz, Chemistry of Materials 21 (2009) 3290–3296.
[28] L. Zhang, C. Xia, F. Zhao, F. Chen, Materials Research Bulletin 45 (2010) 603–608.
[29] S.H. Chan, X.J. Chen, K.A. Khor, Solid State Ionics 158 (2003) 29–43.
[30] Q.L. Liu, K.A. Khor, S.H. Chan, X.J. Chen, Journal of Power Sources 162 (2006) 1036–1042.
[31] F. Zhao, A.V. Virkar, Journal of Power Sources 141 (2005) 79–95.
[32] C.R. Xia, W. Rauch, W. Wellborn, M.L. Liu, Electrochemical and Solid State Letters 5 (2002) A217–A220.
[33] J. Qian, Z. Tao, J. Xiao, G. Jiang, W. Liu, International Journal of Hydrogen Energy 38 (2013) 2407–2412.